Putaminal diffusion tensor imaging measures predict disease severity across human prion diseases

Harpreet Hyare, Enrico De Vita, Marie-Claire Porter, Ivor Simpson, Gerard Ridgway, Jessica Lowe, Andrew Thompson, Chris Carswell, Sebastien Ourselin, Marc Modat, Liane Dos Santos Canas, Diana Caine, Zoe Fox, Peter Rudge, John Collinge, Simon Mead, John S Thornton

BRAIN COMMUNICATIONS

Putaminal diffusion tensor imaging measures predict disease severity across human prion diseases

Harpreet Hyare,[1] Enrico De Vita,[2] Marie-Claire Porter,[1] Ivor Simpson,[3] Gerard Ridgway,[3] Jessica Lowe,[1] Andrew Thompson,[1] Chris Carswell,[1] Sebastien Ourselin,[2] Marc Modat,[2] Liane Dos Santos Canas,[4] Diana Caine,[1] Zoe Fox,[5,6] Peter Rudge,[1] John Collinge,[1] Simon Mead[1] and John S. Thornton[3]

Therapeutic trials of disease-modifying agents in neurodegenerative disease typically require several hundred participants and long durations for clinical endpoints. Trials of this size are not feasible for prion diseases, rare dementia disorders associated with misfolding of prion protein. In this situation, biomarkers are particularly helpful. On diagnostic imaging, prion diseases demonstrate characteristic brain signal abnormalities on diffusion-weighted MRI. The aim of this study was to determine whether cerebral water diffusivity could be a quantitative imaging biomarker of disease severity. We hypothesized that the basal ganglia were most likely to demonstrate functionally relevant changes in diffusivity. Seventy-one subjects (37 patients and 34 controls) of whom 47 underwent serial scanning (23 patients and 24 controls) were recruited as part of the UK National Prion Monitoring Cohort. All patients underwent neurological assessment with the Medical Research Council Scale, a functionally orientated measure of prion disease severity, and diffusion tensor imaging. Voxel-based morphometry, voxel-based analysis of diffusion tensor imaging and regions of interest analyses were performed. A significant voxel-wise correlation of decreased Medical Research Council Scale score and decreased mean, radial and axial diffusivities in the putamen bilaterally was observed ($P < 0.01$). Significant decrease in putamen mean, radial and axial diffusivities over time was observed for patients compared with controls ($P = 0.01$), and there was a significant correlation between monthly decrease in putamen mean, radial and axial diffusivities and monthly decrease in Medical Research Council Scale ($P < 0.001$). Step-wise linear regression analysis, with dependent variable decline in Medical Research Council Scale, and covariates age and disease duration, showed the rate of decrease in putamen radial diffusivity to be the strongest predictor of rate of decrease in Medical Research Council Scale ($P < 0.001$). Sample size calculations estimated that, for an intervention study, 83 randomized patients would be required to provide 80% power to detect a 75% amelioration of decline in putamen radial diffusivity. Putamen radial diffusivity has potential as a secondary outcome measure biomarker in future therapeutic trials in human prion diseases.

1 MRC Prion Unit at UCL, Institute of Prion Diseases, London SE1 7EH, UK
2 Department of Biomedical Engineering, Centre for Medical Engineering, School of Biomedical Engineering & Imaging Sciences, King's College London, King's Health Partners, St Thomas' Hospital, London SE1 7EH, UK
3 UCL Institute of Neurology, London, UK
4 Centre for Medical Image Computing, UCL, London, UK
5 Education Unit, UCL Institute of Neurology, London, UK
6 UCL/UCLH Joint Research Office, London, UK

Correspondence to: Harpreet Hyare, PhD NHS National Prion Clinic, The National Hospital for Neurology & Neurosurgery, Queen Square, Box 98, London C1N 3BG, UK
E-mail: Harpreet.hyare@nhs.net

Received September 24, 2019. Revised December 23, 2019. Accepted December 29, 2019. Advance Access publication April 8, 2020

Keywords: prion; CJD; MRI

Abbreviations: AD = axial diffusivity; DTI = diffusion tensor imaging; FA = fractional anisotropy; GM = grey matter; IPD = inherited prion disease; MD = mean diffusivity; MRC = Medical Research Council; RD = radial diffusivity; ROI = region of interest; sCJD = sporadic Creutzfeldt–Jakob disease; T1w = T_1 weighted; WM = white matter

Graphical Abstract

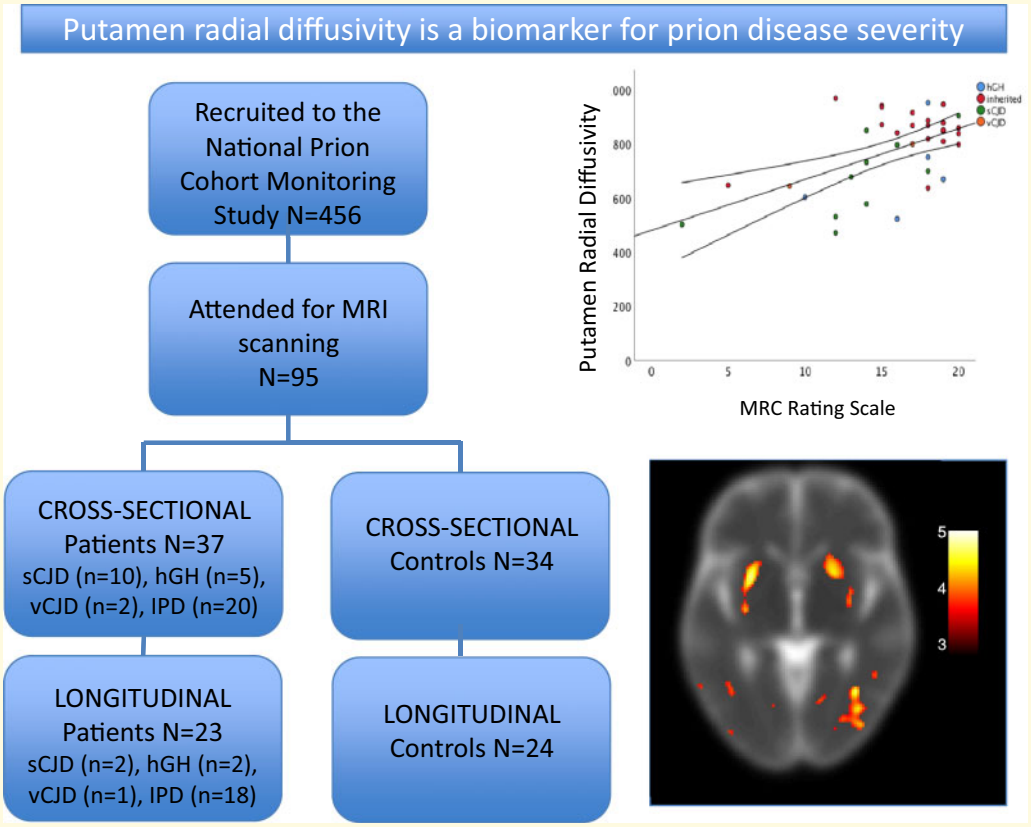

Introduction

Prion diseases are fatal and transmissible neurodegenerative diseases caused by the templated misfolding of prion protein. Most cases occur sporadically with unknown cause, termed sporadic Creutzfeldt–Jakob disease (sCJD), but inherited, iatrogenic, and dietary transmission can also occur. While these aetiological groups share core neuropathological features including spongiform degeneration, gliosis and prion protein deposition, there is marked clinical heterogeneity both within and between them (Jackson and Collinge, 2001).

With preparations for human trials of therapeutic agents (Mead *et al.*, 2016) and compassionate treatments (https://www.uclh.nhs.uk/News/Pages/FourthUCLHpatientt obegiveninnovativetreatmentforCJD.aspx), there is a need for responsive outcome measures applicable in the practically available patient cohorts. The Medical Research Council Prion Disease Rating Scale (MRC Scale) (Thompson *et al.*, 2013) that captures neurological, cognitive and functional disease features, giving an overall measure of severity, was recently developed and optimized for this specific application. The purpose of the current work was to evaluate the potential of magnetic resonance brain diffusion tensor imaging (DTI) to provide objective secondary measures of disease progression (biomarkers) complementing this subjective clinical rating scale.

The sensitivity of cerebral diffusion-weighted imaging to prion disease pathology is well established (Kropp *et al.*, 2000; Matoba *et al.*, 2001; Shiga *et al.*, 2004; Young *et al.*, 2005; Meissner *et al.*, 2008; Vitali *et al.*, 2011; Suzuki *et al.*,2016; Zanusso *et al.*, 2016; Iwasaki *et al.*, 2017). Orthogonal-diffusion direction-sensitized quantitative diffusion-weighted imaging has shown that, in sCJD caudate, putamen and thalamus (Tschampa *et al.*, 2003; Hyare *et al.*, 2010) and rolandic cortex (Lin *et al.*, 2006), signal abnormalities are due to decreased mean diffusivity (MD). Serial measurements in sCJD have shown both progressive striatal MD decrease (Murata

et al., 2002; Eisenmenger *et al.*, 2016) and basal ganglia MD increase (Tschampa *et al.*, 2003), suggesting a disease-stage-dependent MD trajectory.

A limited number of studies have obtained DTI from patients with prion disease, yielding per-voxel estimates of the self-diffusion tensor eigenvalues (λ_1, λ_2, λ_3), which may be combined to compute summary metrics including the MD, fractional anisotropy (FA), reflecting the directional dependence of water self-diffusion, and λ_1 and $\frac{\lambda_1+\lambda_2}{2}$, commonly referred to respectively as the axial diffusivity (AD) and RDs in white matter (WM) regions. These indices are established markers of brain tissue microstructural change: for instance in normal ageing, WM MD increases and FA decreases, especially in the genu of the corpus callosum and prefrontal WM (Nusbaum *et al.*, 2001; Abe *et al.*, 2002; Sullivan *et al.*, 2006), while in striatal grey matter (GM), MD decrease is accompanied by a decrease in FA reflecting decreased $\frac{\lambda_1+\lambda_2}{2}$ (Lebel *et al.*, 2008; Wang *et al.*, 2010).

Small-series or case-study reports have suggested the value of cerebral DTI metrics in sCJD (Fujita *et al.*, 2008; Grau-Rivera *et al.*, 2016*a*). Cross-sectional data in sCJD (Caverzasi *et al.*, 2014*a*, *b*) and a mixed sCJD and inherited prion disease (IPD) cohort (Grau-Rivera *et al.*, 2016*b*) demonstrated reduced MD in various WM regions and deep GM nuclei in sCJD, and cross-sectional WM tract MD reduction. Longitudinal follow-up in a small sCJD group (Caverzasi *et al.*, 2014*a*) suggested that MD trajectory was not monotonic with time but tended to decrease initially before later increasing, supporting the hypothesis of a disease-stage-dependent MD trajectory.

In a large cohort of patients symptomatic with various forms of prion disease, we first compared single time-point DTI measurement group-wise between patients and healthy controls and, in symptomatic patients, correlated DTI measures with disease severity rated according to the MRC Scale. Second, in a subset of individuals studied longitudinally, the rate of change with time in DTI measures was compared between patient and control groups and, for the patients, correlated with the monthly rate of change in MRC Scale score. In the light of previous investigations (Murata *et al.*, 2002; Tschampa *et al.*, 2013; Eisenmenger, 2016), we hypothesized that the basal ganglia were most likely to demonstrate functionally relevant longitudinal diffusivity changes.

Materials and methods

Subjects

A total of 71/456 consecutive individuals (21%) recruited to the National Prion Cohort Monitoring Study over a 4-year period attended for MRI (Fig. 1) (Thompson *et al.*, 2013). Ethical approval for the study was granted by the Eastern Multicentre Research Ethics Committee, and informed consent for participation was given either by the patient or by their next of kin. There were 37 symptomatic individuals with a clinical diagnosis of prion disease (patients) and 34 age-matched healthy individuals (control) (Table 1). Diagnosis of 'patients' involved established diagnostic criteria; we included patients with both probable (n = 19) and definite (n = 28) diagnoses. Of the 37 'patients', the diagnoses were sCJD (n = 10), iatrogenic prion disease consequent to exposure to cadaver-derived human growth hormone (CJD) (n = 5), variant Creutzfeldt–Jakob disease (n = 2) and IPD (n = 20). *PRNP* analysis confirmed the causal mutation in IPD: P102L (n = 7), Y163X (n = 3), 5-OPRI (n = 3), 6-OPRI (n = 3), A117V (n = 2), E200K (n = 1), D178N (n = 1). Forty-seven of these subjects underwent serial scanning (Table 2) with a mean duration of 16.2 ± 6.3 months for 'controls' and 14.2 ± 10.3 months for 'patients' (sCJD 5.1 months, human growth hormone-acquired CJD 2.9 months, IPD 20.1 months). The mean duration of symptoms at the time of the first MRI was 2.9 ± 1.2 months for 'patients' (sCJD 1.3 months, human growth hormone CJD 0.6 months, IPD 3.3 months).

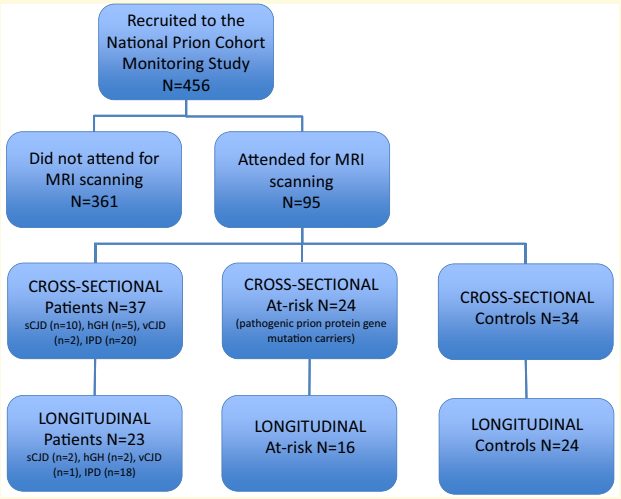

Figure 1 Flow chart describing the recruitment of individuals into the study. Ninety-five participants attended for MRI scanning: 37 patients and 34 controls. Twenty-three patients and 24 controls underwent serial scanning. hGH = human growth hormone; vCJD = variant Creutzfeldt–Jakob disease.

Neurological investigation

All participants underwent systematic neurological and rating scale assessments including the MRC Scale (Thompson *et al.*, 2013) giving an overall measure of disease severity from 20 (un-impaired) to 0 (very severely impaired), performed on the same day as MRI.

MRI acquisition

MRI at 3T (Siemens Tim Trio) included T_1-weighted (T_1w) structural images [3D-magnetization-prepared rapid

acquisition with gradient echo (MPRAGE); repetition time/echo time/inversion time 2200/2.9/900 ms, flip angle 10°, 208 1.1 mm sagittal partitions, field of view (28.2 cm)^2, matrix 256 × 256]. For echo-planar DTI, 75 trans-axial slices of thickness 2.0 mm with diffusion-weighting b value = 1000 s mm^{-2} in 64 directions were acquired [repetition time/echo time 9500/93 ms, field of view (19.2 cm)^2, matrix 96 × 96, 1 average] with 8 acquisitions with b value = 0 s mm^{-2}.

Table 1 Cross-sectional group data including DTI measure region of interest values

	A: controls (n = 34)	B: patients (n = 37)	P-value$^+$
Age (years)	48.7 (13.0)	50.7 (10.4)	0.29
MRC Scale	20 (0)	15.7 (4.1)	<0.001
Male gender	15	20	0.44
TIV (ml)	1.58 (0.17)	1.59 (0.18)	0.73
MD (×10^{-6} mm^2 s^{-1})			
Caudate	952.7 (100.1)	953.0 (229.7)	0.45
Putamen	713.9 (44.1)	666.4 (135.8)	0.03
Thalamus	856.6 (53.5)	930.2 (164.7)	0.01
FA			
Caudate	0.22 (0.04)	0.19 (0.03)	<0.01
Putamen	0.25 (0.04)	0.24 (0.04)	NS
Thalamus	0.29 (0.03)	0.26 (0.04)	<0.01
RD (×10^{-6} mm^2 s^{-1})			
Caudate	980.7 (161.2)	997.6 (297.0)	0.21
Putamen	842.7 (38.2)	775.9 (140.8)	<0.01
Thalamus	983.5 (86.6)	1032.4 (165.2)	0.68
AD (×10^{-6} mm^2 s^{-1})			
Caudate	1148.6 (161.01)	1147.6 (296.2)	0.29
Putamen	945.1 (42.8)	875.3 (165.6)	0.01
Thalamus	1114.0 (92.0)	1158.2 (201.1)	0.38

Values for continuous measures are mean (standard deviation).
+ = Kruskal–Wallis test.
NS = not significant; TIV = total intracranial volume.

Image data preprocessing

Spatial processing for voxel-based morphometry was performed for T_1w structural images using SPM Version 8 software (SPM8; http://www.fil.ion.ucl.ac.uk/spm: (i) WM versus GM segmentation using SPM8's unified approach, which combines segmentation, bias field correction and normalization to the Montreal Neurological Institute space into a single generative model (Ashburner and Friston, 2005). Registration across images was used to produce approximately aligned images for the following step: (ii) generation of a cohort-specific template for GM and WM segments using DARTEL (Ashburner, 2007); (iii) warping and resampling of individual GM and WM segments to the cohort-specific template. For voxel-based morphometry, local intensities were multiplied by the ratio of voxel volume (before and after normalization) to account for normalization-associated volume changes; (iv) an isotropic 6 mm full-width-at-half-maximum Gaussian kernel was applied to the GM and WM datasets; and (v) an 'objective' masking strategy (Ridgway *et al.*, 2009) was employed to define the voxels for subsequent statistical analysis on GM and WM segments separately. Total intracranial volume was estimated as the sum of the GM, WM and CSF segments.

Table 2 Longitudinal analysis: group-wise rates-of-change in MRC Scale score and ROI DTI measures

	A: controls (n = 24)	B: patients (n = 23)	P-value,[a] A versus B
Age at entry (years), mean (SD)	48.9 (12.1)	49.0 (8.8)	0.22
Time between symptom onset and first MRI (months), mean (SD)		2.9 (1.2)	
Time between first and last MRI (months), mean (SD)	16.2 (6.7)	14.2 (10.5)	0.26
Male gender	12	13	0.73
Neurological outcomes			
MRC Scale score change-per-month, median (IQR, interquartile range)	0.0 (0.0–0.0)	−0.26 (−0.60 to −0.10)	<0.0001
DTI metrics			
MD rate of change (×10^{-6} mm^2 s^{-1} month^{-1}) mean (95% CI)			
Caudate ROI	0.31 (−0.72 to 1.34)	0.63 (−6.61 to 7.87)	0.86
Putamen ROI	−0.87 (−1.74 to 0.01)	−6.82 (−12.06 to −1.58)	0.01
Thalamus ROI	−0.81 (−1.85 to 0.24)	−0.77 (−9.08 to 7.54)	0.99
FA rate of change (×10^3 month^{-1}) mean (95% CI)			
Caudate ROI	0.16 (−0.33 to 0.64)	0.68 (−0.42 to 1.78)	0.60
Putamen ROI	0.34 (−0.17 to 0.84)	2.53 (0.16 to 4.89)	0.06
Thalamus ROI	0.47 (−0.11 to 1.05)	0.07 (−3.76 to 3.90)	0.97
RD rate of change (×10^{-6} mm^2 s^{-1} month^{-1}) mean (95% CI)			
Caudate ROI	0.21 (−0.85 to 1.26)	0.48 (−6.31 to 7.27)	0.86
Putamen ROI	−0.88 (−1.76 to 0.00)	−7.04 (−12.07 to −2.00)	0.008
Thalamus ROI	−0.89 (−1.93 to 0.16)	−0.51 (−8.92 to 7.89)	0.99
AD rate of change (×10^{-6} mm^2 s^{-1} month^{-1}) mean (95% CI)			
Caudate	0.51 (−0.53 to 1.55)	0.94 (−7.29 to 9.18)	0.86
Putamen ROI	−0.85 (−1.79 to 0.08)	−6.38 (−12.30 to −0.47)	0.05
Thalamus ROI	−0.65 (−1.70 to 0.41)	−1.28 (−9.47 to 6.91)	0.96

[a]ANOVA. + = Kruskal-Wallis test.
CI = confidence intervals; SD = standard deviation.

The FDT tool in FSL (Jenkinson *et al.*, 2002) was used to process the raw DTI data providing motion and eddy-current gradient distortion correction before the generation of MD, FA, RD and AD maps. DTI-voxel based analysis (VBA) data preprocessing involved: (i) affine transformation between each DTI dataset and the corresponding T_1w images estimated with 'reg3d' (Modat *et al.*, 2010) to partially correct geometric distortion associated with EPI acquisition; (ii) combination of these transforms with the warps computed for the T_1w data to normalize (with 'no' modulation) individual MD, FA, RD and AD maps to the cohort T_1w template generated for voxel-based morphometry; (iii) 6 mm smoothing; and (iv) mask generation by summing GM and WM masks from voxel-based morphometry.

Region of interest definition

Bilateral region of interests (ROIs) were drawn on the average warped and smoothed T1w volumes in the thalamus, head of caudate and putamen and verified by an experienced neuroradiologist on the averaged smoothed datasets to ensure that the smoothing did not cause CSF contamination. For patients who underwent serial imaging, six ROIs encompassing the caudate, putamen and thalamus bilaterally were segmented through the propagation of anatomical labels from a set of 35 expertly annotated T1w images (Neuromorphometrics Inc., Somerville, MA, USA). The set of labelled images was registered to each subject image using Niftyreg (Modat *et al.*, 2010). The final labelled areas were estimated by majority voting of the registered labels (Heckemann *et al.*, 2006). The DTI metrics were extracted by transferring such ROIs to the DTI space using the nearest-neighbour interpolation (Ryan *et al.*, 2013).

Statistical analysis

Cross-sectional group comparison

'Clinical': differences in age, sex, total intracranial volume and MRC score were assessed using the Kruskal–Wallis test. 'ROI analysis': right versus left asymmetry for all ROIs across all subject groups for all MRI parameters was assessed using the paired *t*-test and no significant differences were observed (for example right caudate MD 939 ± 120 versus left caudate MD 947 ± 138 mm^2 s^{-1}, $P = 0.28$; right putamen MD 715 ± 49 versus left putamen MD 741 ± 49 mm^2 s^{-1}, $P = 0.27$; right thalamus MD 862 ± 81 versus left thalamus MD 892 ± 77 mm^2 s^{-1}, $P = 0.10$). Therefore, the left and right ROI mean values were combined providing an ROI average from each of the caudate, putamen and thalamus for each dataset. Differences in ROI parameters between subject groups and the largest subgroups (IPD and sCJD) were assessed using the Kruskal–Wallis test.

Cross-sectional correlation with MRC Scale score

'DTI-VBA': in the 'patients', we assessed correlations between MRC Scale and GM, WM, MD, FA, RD and AD separately, by voxel-wise linear regression with individual age and total intracranial volume as covariates. 'SPM'-t maps were produced using a $P < 0.01$ level of significance after multiple comparison correction using false discovery rate. 'ROI analysis': associations between baseline putaminal ROI mean MD, FA, RD and AD and MRC Scale score in individual 'patients' were investigated graphically and by Pearson correlation coefficient.

Longitudinal ROI analysis

Linear regression was performed across all of the available time points to model for each subject the change-per-month for, separately, the MRC Scale score and the DTI ROI average measures, after plotting the values over time and noting a linear trend. The time origin for each subject was defined as the time of their first scan. MRC Scale score and DTI measure rates-of-change were compared between groups using ANOVA, with $P < 0.05$ considered as statistically significant. For the 'patients', unadjusted and adjusted multilevel mixed-effects models were used to investigate factors associated with the rate of change in MRC score. Age, sex, disease duration and *PRNP* polymorphic codon 129 were included as covariates.

Sample size calculation

Finally, sample size calculations were performed for a hypothetical trial of an intervention expected to ameliorate the monthly rate of decline for each MRI measure by 50%, 75% and 90%, with the primary outcome of a difference in mean between the intervention and placebo groups. The sample size calculation, using standard equations for a difference in means, was performed using the 'sampsi' command in the statistical software Stata (version 13.1).

Data availability

The imaging data used in this study are available on request to the corresponding author.

Results

Subjects

Details of the subjects recruited to the trial and those included in the cross-sectional and longitudinal analysis reported here are given in Fig. 1.

Cross-sectional group-wise comparisons

Clinical

There were no significant group differences in age, gender or total intracranial volume between 'patients' and 'controls'. MRC Scale scores within the 'patients' group ranged from 2 to 20, while all 'controls' had an MRC Scale score of 20 ($P < 0.001$, 'patients' versus 'controls') (Table 1).

ROI analysis

These data are summarized in Table 1. Putamen MD, putamen RD and putamen AD were significantly lower in 'patients' compared to 'controls'. Thalamus MD was significantly higher in 'patients' compared to 'controls' (thalamus MD 856.6 ±53.5 versus 930.2 ±164.7 mm^2 s^{-1}, $P =< 0.01$). Significantly lower FA was seen in caudate and thalamus ROIs for 'patients' compared to 'controls'.

In the sCJD subgroup ($n = 10$), significantly reduced putamen AD, MD and RD were observed compared to controls (Supplementary Table 1). However, for the IPD subgroup ($n = 20$), there were no significant differences observed in the putamen ROI for each of the parameters (Supplementary Table 1).

Cross-sectional correlation with MRC score

Voxel-wise analysis

A significant positive correlation with MRC Scale was seen in the putamen bilaterally for MD, RD and AD: decreased MRC Scale correlated with decreased MD, RD and AD (Fig. 2). There were no regions of negative correlation between MRC score and MD, RD and AD. There were no significant correlations of MRC Scale with GM, WM or FA in either direction.

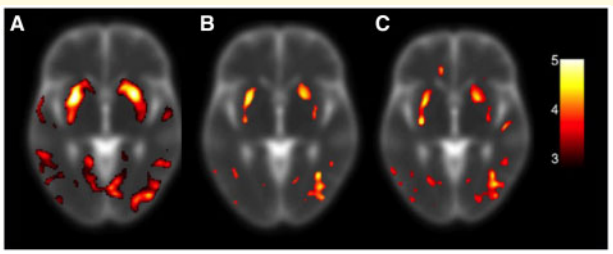

Figure 2 Cross-sectional VBA correlation of DTI measures with MRC Scale in 'patients'. SPM-t maps showing significant positive correlation between MRC Scale and DTI metrics in the putamen bilaterally in 'patients' ($n = 37$) for FDR $P < 0.05$: (**A**) MD, $t \geq 2.823$, $r = 0.57$; (**B**) RD, $t \geq 3.61$, $r = 0.46$ and (**C**) AD, $t \geq 3.321$, $r = 0.54$. Colour scale $t = 2.8$–5.0. FDR = false discovery rate.

ROI analysis

Putamen ROI MD, RD and AD each correlated significantly with MRC Scale ($P < 0.01$), Fig. 3A–D, confirming the voxel-wise analysis findings. The strongest correlation with MRC Scale was observed for putamen MD ($r = 0.57$, $P < 0.01$) followed by AD and RD. The subgroup analysis confirmed the significant correlations in both the IPD (IPD: putamen AD $r = 0.58$, $P < 0.01$; putamen MD $r = 0.62$, $P < 0.01$, putamen RD $r = 0.58$, $P < 0.01$) and sCJD subgroups (sCJD: putamen AD $r = 0.68$, $P = 0.03$; putamen MD $r = 0.67$, $P = 0.03$, putamen RD $r = 0.69$, $P = 0.03$).

Longitudinal ROI analysis

Longitudinal data were available for 23 'patients' (2 sCJD, 2 human growth hormone CJD, 1 variant Creutzfeldt–Jakob disease, 18 IPD, 15 males, mean age 48.5 ± 8.7 years; mean final follow-up 14.2 ± 10.3 months) and 24 'controls' (12 males, mean age 48.5 ± 12.2 years, mean final follow-up 16.2 ± 6.3 months). The group mean rates-of-change in DTI metrics in each ROI are given in Table 2 with the rates-of-change in MRC Scale.

Significant differences in DTI-metric rates-of-change between groups were observed in the putamen, but not in any other ROI. The mean rate of change for 'patients' was as follows: −6.82 (95% CI −12.06 to −1.58) × 10^{-6} mm^2 s^{-1} $month^{-1}$, −7.04 (95% CI −12.07 to −2.00) mm^2 s^{-1} $month^{-1}$ and −6.38 (95% CI −12.30 to −0.47) × 10^{-6} mm^2 s^{-1} $month^{-1}$ for putamen MD, RD and AD respectively. The rate of increase in putamen FA in 'patients' was [2.53 (95% CI 0.16 to 4.89)].

A significant positive correlation was observed between the rate of change in putamen MD, RD and AD and rate of change in MRC Scale in the 'patients' ($P < 0.001$).

The step-wise linear regression showed that change in putamen RD was a marginally stronger predictor of rate of MRC Scale change than putamen MD or AD. The adjusted mean (95% CI) putamen rates-of-change were for RD −0.88 (−1.76 to 0.00) × 10^{-6} mm^2 s^{-1} $month^{-1}$ ($P = 0.008$), for MD −0.87 (−1.74 to 0.01) × 10^{-6} mm^2 s^{-1} $month^{-1}$, $P = 0.01$ and for AD slope −0.85 (−1.79 to 0.08) × 10^{-6} mm^2 s^{-1} $month^{-1}$ ($P = 0.05$).

Sample size calculation for a hypothetical intervention study

Sample size calculations estimated that, to provide 80% power to detect a true amelioration in mean decline in slope for putamen MD of 50%, 75% and 90%, 216, 96 and 67 patients, respectively, would be needed per arm for an intervention study, while for putamen RD, 186, 83 and 58 patients per arm would be required, respectively, to detect the same true changes, and for putamen AD, respectively, 310, 138 and 96 patients.

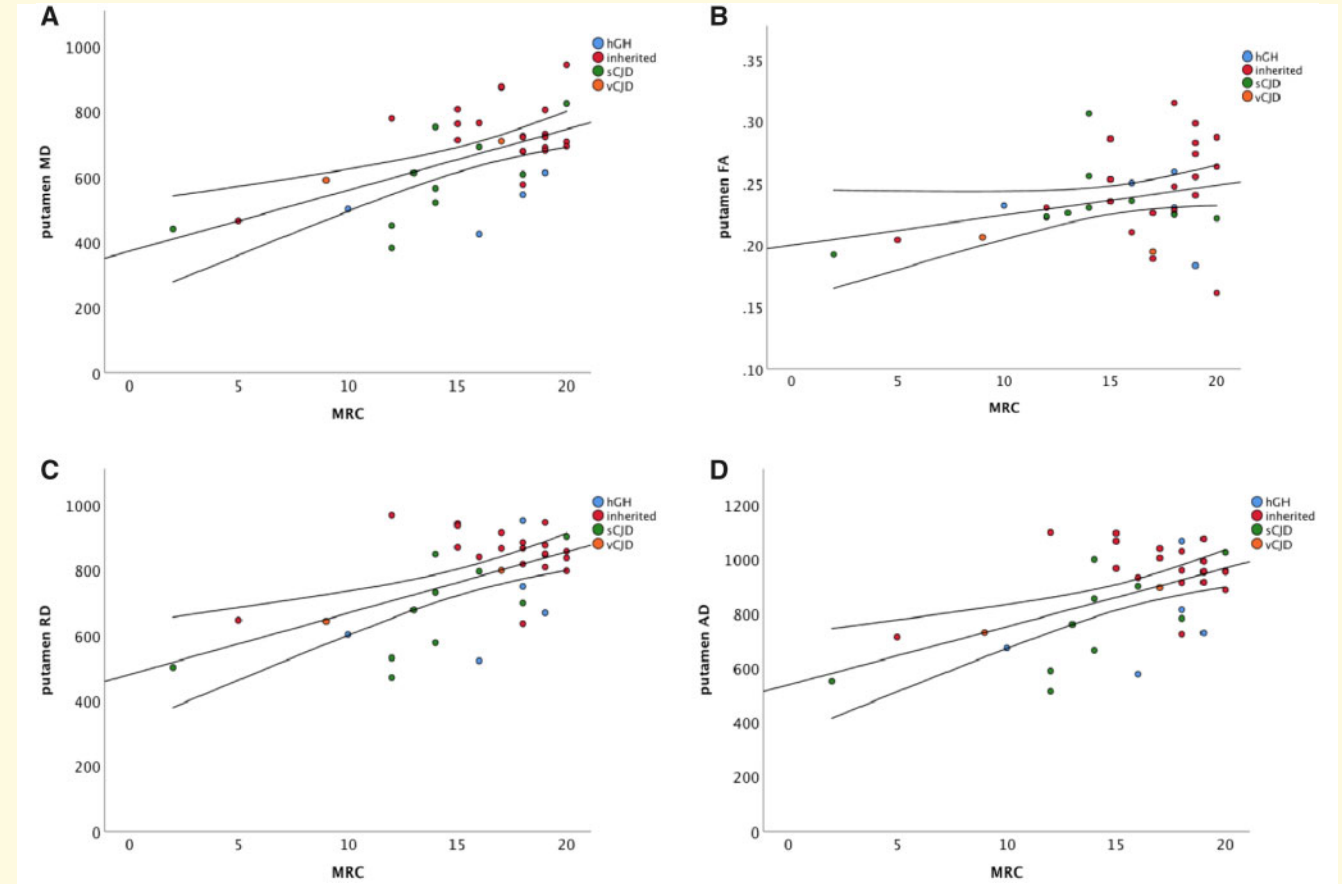

Figure 3 Cross-sectional correlation of DTI metrics with MRC Scale in the putamen. Graphs show scatterplots of DTI metrics versus MRC Scale with line of best fit and 95% confidence intervals. (**A**) MD, $r = 0.57$, $P < 0.01$, (**B**) FA $r = 0.29$, $P = 0.4$, (**C**) RD, $r = 0.46$, $P < 0.01$ and (**D**) AD, $r = 0.54$, $P < 0.01$. hGH = human growth hormone; vCJD = variant Creutzfeldt–Jakob disease.

Discussion

In a large cohort with various forms of human prion disease, we have investigated cross-sectional and longitudinally obtained cerebral DTI metrics as potential biomarkers. We have shown that despite the clinical and imaging heterogeneity of patients with human prion diseases, by focusing on a key anatomical region across all patients, DTI measures (MD, RD and AD) correlate with functional scores of disease severity both at baseline and over time, with change in RD being a marginally stronger predictor of change in disease severity. Putamen diffusion measures have potential as secondary outcome readouts in future therapeutic trials in human prion diseases.

A limitation of this work is the heterogeneity of the patient sample. Prion diseases are highly heterogeneous conditions, including the most common aetiological subtype sCJD, which has a number subtypes with markedly different clinical courses and neuropathology (Parchi *et al.*, 1999; Mead *et al.*, 2016). The most common type of sCJD that might potentially provide the sample sizes needed for an adequately powered study is associated with *PRNP* codon 129 genotype MM and type 1 PrP^{Sc} and comprises 65% of the annual incidence; however, this is the most rapidly disabling form and no centre has yet been able to achieve the recruitment of this subtype to longitudinal study. Therefore, this field of work for the time being must contend with the aetiological heterogeneity of disease, while accepting shared aspects of the pathogenesis and neuropathology. Despite this disease heterogeneity, the reported correlation was maintained in the subgroup analysis performed separately for sCJD and IPD, suggesting that one subgroup was not driving the reported findings and that the shared histopathology of spongiosis, gliosis and prion protein deposition are driving the MRI signal changes.

Our findings of significantly reduced MD in the putamen are in line with previous reports that have measured MD in sCJD (Tschampa *et al.*, 2003; Lin *et al.*, 2006; Hyare *et al.*, 2010; Grau-Rivera *et al.*, 2016*b*). It is surprising that reduced caudate and thalamus MD was not detected in this study, possible due to partial voluming artefact from adjacent CSF. This is the first study to show a significant correlation of reduced MD in the

putamen with disease severity. Decreased MD in the striatum over 2 weeks has been previously reported (Murata *et al.*, 2002) while other studies report an increase in basal ganglia MD values with time, suggesting that MD may vary according to the stage of disease (Tschampa, 2003; Caverzasi, 2014*a*). In IPD, a study of patients with the six-OPRI mutation demonstrated no significant MD differences in the basal ganglia between patients and controls (De Vita *et al.*, 2013), whereas in a cohort of patients with the E200K mutation, decreased MD in the basal ganglia was seen 'before' symptom onset suggesting that MD measurements could be used for the timing of therapeutic interventions (Lee *et al.*, 2009). Our findings of a significant decrease in putamen MD in symptomatic patients compared to controls over time confirm these reports while our use of the disease-optimized MRC Scale may have enabled us to identify cross-sectional correlations between DTI measures and clinical severity not found in a previous study (Caverzasi *et al.*, 2014). While we acknowledge that some of the items in the MRC Scale detect basal ganglia dysfunction, there are several other items including bowel and bladder function that do not. We studied patients with relatively early disease, who would be good candidates for therapeutic trials and who were fit enough to travel to our centre. We did not study many patients in the very advanced stages of disease (MRC Scale 0–10) when biomarker trajectories have been hypothesized to alter direction.

While previous studies have reported changes in the DTI-determined summary measures FA in human prion diseases, we found that consideration of the putamen tensor eigenvalues, reported here in terms of the so-called RDs and ADs, provided additional sensitivity with respect to correlation with disease severity both cross-sectionally and longitudinally. In WM tracts, interpretation of RD and AD is straightforward in terms of water diffusing faster along the direction parallel to the axons (AD) than in directions perpendicular to the axons (RD). The geometric interpretation of these measures in tissue regions such as deep GM, lacking simple cylindrical symmetry at the microscopic level, is less certain. Neurons in the basal ganglia have a spheric dendritic arborization, which is covered densely with dendritic spines allowing water to diffuse more freely in all directions (Beaulieu, 2002).

Severe spongiform change with areas of confluent vacuolation, restricting the extracellular space, has been advocated as a potential cause of decreased MD (Murata *et al.*, 2002; Mittal *et al.*, 2002; Lim *et al.*, 2004; Eisenmenger, 2016). One would expect diffusion to be affected equally in all directions, and it is interesting therefore that decreased RD was a marginally stronger predictor of worsening disease severity. Decreased MD in the caudate and putamen is also seen with ageing in healthy subjects (Wang *et al.*, 2010) in contrast to increasing MD in WM. Those authors suggest that concurrent gliosis and tissue compaction with ageing contribute to the decreased basal ganglia MD. The putamen is a region of the brain with abundant blood supply compared to other regions of the brain. The vessel walls experience hyaline degeneration with age so that water diffusion through the vessel wall becomes more difficult, contributing to reduced RD with age (Wang *et al.*, 2010). It is possible that disease-associated prion protein deposition in vessel walls (Ghetti *et al.*, 1996; Koperek *et al.*, 2002) contributes to reduced RD in the putamen in human prion diseases. Alternatively, RD may simply provide a statistically more robust measure of prion disease micro-pathology being the mean of two generally closely similar eigenvalues. Future diffusion imaging studies using more sophisticated acquisition schemes and model-driven analysis (Zhang *et al.*, 2012) may shed more light on the microstructural substrates of the changes we observed.

In the prospect of clinical trials for prion disease, it is likely that functionally orientated scales will be used in rapidly progressive patients (Thompson *et al.*, 2013). While only two sCJD patient data sets were available for our longitudinal analysis, the longitudinal results were entirely consistent with our cross-sectional analysis in a larger patient group with sCJD cases more strongly represented. Our results imply that for a reasonably sized two arm study, an intervention would need to provoke an °75% true change in monthly rate of decline in putamen MD or RD to be detected with reasonable power. This relatively low sensitivity may be due in part to the heterogeneous types of prion disease patients that we were able to recruit for this study. Clinically sCJD patients deteriorate much more rapidly than the other prion disease subgroups, and our data support the hypothesis that, in an sCJD only trial, putamen RD may provide a responsive secondary endpoint. The scope of these analyses could not take into account a range of additional factors that might influence power in the range of potential future clinical trial designs.

In conclusion, this is the largest cross-sectional and longitudinal study correlating DTI metrics with prion disease severity. Overall, the results confirm that, despite the clinical and imaging heterogeneity of patients affected by human prion diseases, the putamen, with its rich connectivity, appears to be a key anatomical structure where reduced MD, RD and AD correlate with disease severity. Reduced RD was marginally the strongest predictor of decline in disease severity, possibly due to a combination of spongiosis, microglial proliferation and disease-associated prion protein deposition in vessel walls.

Supplementary material

Supplementary material is available at *Brain Communications* online.

Funding

The National Prion Monitoring Cohort study was originally funded by the Department of Health (England) and is now supported by the National Institute for Health Research University College London Hospitals Biomedical Research Centre. Additional support was provided by the UK Medical Research Council. This study supported by the National Institute for Health Research University College London Hospitals Biomedical Research Centre. E.D.V. is supported by the Wellcome/Engineering and Physical Science Research Council (EPSRC) Centre for Medical Engineering [WT 203148/Z/16/Z].

Competing interests

The authors report no competing interests.

References

Abe O, Aoki S, Hayashi N, Yamada H, Kunimatsu A, Mori H, et al. Normal aging in the central nervous system: a quantitative MR diffusion-tensor analysis. Neurobiol Aging 2002; 23: 433–41.

Ashburner J, Friston KJ. Unified segmentation. NeuroImage 2005; 26: 839–51.

Ashburner J. A fast diffeomorphic image registration algorithm. NeuroImage 2007; 38: 95–113.

Beaulieu C. The basis of anisotropic water diffusion in the nervous system—a technical review. NMR Biomed 2002; 15: 435–55.

Caverzasi E, Henry RG, Vitali P, Lobach IV, Kornak J, Bastianello S, et al. Application of quantitative DTI metrics in sporadic CJD. Neuroimage Clin 2014a; 4: 426–35.

Caverzasi E, Mandelli ML, DeArmond SJ, Hess CP, Vitali P, Papinutto N, et al. White matter involvement in sporadic Creutzfeldt–Jakob disease. Brain 2014b; 137 (Pt 12): 3339–54

De Vita E, Ridgway GR, Scahill RI, Caine D, Rudge P, Yousry TA, et al. Multiparameter MR imaging in the 6-OPRI variant of inherited prion disease. AJNR Am J Neuroradiol 2013; 34: 1723–30

Eisenmenger L, Porter MC, Carswell CJ, Thompson A, Mead S, Rudge P, et al. Evolution of diffusion-weighted magnetic resonance imaging signal abnormality in sporadic Creutzfeldt–Jakob disease, with histopathological correlation. JAMA Neurol 2016; 73: 76–84.

Fujita K, Nakane S, Harada M, Izumi Y, Kaji R. Diffusion tensor imaging in patients with Creutzfeldt–Jakob disease. J Neurol Neurosurg Psychiatry 2008; 79: 1304–6.

Ghetti B, Piccardo P, Spillantini MG, Ichimiya Y, Porro M, Perini F, et al. Vascular variant of prion protein cerebral amyloidosis with tau-positive neurofibrillary tangles: the phenotype of the stop codon 145 mutation in PRNP. Proc Natl Acad Sci USA 1996; 93: 744–8.

Grau-Rivera O, Calvo A, Bargalló N, Monté GC, Nos C, Lladó A, et al. Quantitative magnetic resonance abnormalities in Creutzfeldt–Jakob disease and fatal insomnia. J Alzheimers Dis 2016a; 55: 431–43.

Grau-Rivera O, Sánchez-Valle R, Bargalló N, Lladó A, Gaig C, Nos C, et al. Sporadic MM2-thalamic + cortical Creutzfeldt–Jakob disease: utility of diffusion tensor imaging in the detection of cortical involvement in vivo. Neuropathology 2016b; 36: 199–204.

Heckemann RA, Hajnal JV, Aljabar P, Rueckert D, Hammers A. Automatic anatomical brain MRI segmentation combining label propagation and decision fusion NeuroImage 2006; 33: 115–26.

Hyare H, Thornton J, Stevens J, Mead S, Rudge P, Collinge J, et al. High-b-value diffusion MR imaging and basal nuclei apparent diffusion coefficient measurements in variant and sporadic Creutzfeldt–Jakob disease. Am J Neuroradiol 2010; 31: 521–6.

Iwasaki Y, Mori K, Ito M, Mimuro M, Kitamoto T, Yoshida M. An autopsied case of MM1 + MM2-cortical with thalamic-type sporadic Creutzfeldt–Jakob disease presenting with hyperintensities on diffusion-weighted MRI before clinical onset. Neuropathology 2017; 37: 78–85.

Jackson GS, Collinge J. The molecular pathology of CJD: old and new variants. Mol Pathol 2001; 54: 393–9.

Jenkinson M, Bannister P, Brady M, Smith S. Improved optimization for the robust and accurate linear registration and motion correction of brain images. NeuroImage 2002; 17: 825–41.

Koperek O, Kovacs GG, Ritichie D, Ironside JW, Budka H, WIck G. Disease-associated prion protein in vessel walls. Am J Pathol 2002: 161: 1979–84.

Kropp S, Finkenstaedt M, Zerr I, Schroter A, Poser S. Diffusion-weighted MRI in patients with Creutzfeldt–Jakob disease. Nervenarzt 2000; 71: 91–5.

Lebel C, Walker L, Leemans A, Phillips L, Beaulieu C. Microstructural maturation of the human brain from childhood to adulthood. NeuroImage 2008; 40: 1044–55.

Lee H, Rosenmann H, Chapman J, Kingsley PB, Hoffmann C, Cohen OS, et al. Thalamo-striatal diffusion reductions precede disease onset in prion mutation carriers. Brain 2009; 132 (Pt 10): 2680–7.

Lee H, Cohen OS, Rosenmann H, Hoffmann C, Kingsley PB, Korczyn AD, et al. Cerebral white matter disruption in Creutzfeldt–Jakob disease. AJNR Am J Neuroradiol 2012; 33: 1945–50.

Lin YR, Young GS, Chen NK, Dillon WP, Wong S. Creutzfeldt–jakob disease involvement of rolandic cortex: a quantitative apparent diffusion coefficient evaluation. AJNR Am J Neuroradiol 2006; 27: 1755–9.

Lim CC, Tan K, Verma KK, Yin H, Venketasubramanian N. Combined diffusion-weighted and spectroscopic MR imaging in Creutzfeldt–Jakob disease. Magn Reson Imaging 2004; 22: 625–9.

Matoba M, Tonami H, Miyaji H, Yokota H, Yamamoto I. Creutzfeldt–Jakob disease: serial changes on diffusion-weighted MRI. J Comput Assist Tomogr 2001; 25: 274–77.

Mead S, Burnell M, Lowe J, Thompson A, Lukic A, Porter MC, et al. Clinical trial simulations based on genetic stratification and the natural history of a functional outcome measure in Creutzfeldt–Jakob disease. JAMA Neurol 2016; 73: 447–55.

Meissner B, Kallenberg K, Sanchez-Juan P, Krasnianski A, Heinemann U, Varges D, et al. Isolated cortical signal increase on MR imaging as a frequent lesion pattern in sporadic Creutzfeldt–Jakob disease. AJNR Am J Neuroradiol 2008; 29: 1519–24.

Mittal S, Farmer P, Kalina P, Kingsley PB, Halperin J. Correlation of diffusion-weighted magnetic resonance imaging with neuropathology in Creutzfeldt–Jakob disease. Arch Neurol 2002; 59: 128–34.

Modat M, Ridgway GR, Taylor ZA, Lehmann M, Barnes J, Hawkes DJ, et al. Fast free-form deformation using graphics processing units. Comput Methods Programs Biomed 2010; 98: 278–84.

Murata T, Shiga Y, Higano S, Takahashi S, Mugikura S. Conspicuity and evolution of lesions in Creutzfeldt–Jakob disease at diffusion-weighted imaging. AJNR Am J Neuroradiol 2002; 23: 1164–72.

Nusbaum AO, Tang CY, Buschbaum MS, Wei TC, Atlas SW. Regional and global changes in cerebral diffusion with normal aging. AJNR Am J Neuroradiol 2001; 22: 136–42.

Ourselin S, Roche A, Subsol G, Pennec X, Ayache N, Reconstructing a serial structure from serial histological sections. Image Vision Comput 2001; 19: 25–31.

Parchi P, Giese A, Capellari S, Brown P, Schulz-Schaeffer W, Windl O, et al. Classification of sporadic Creutzfeldt–Jakob disease based on molecular and phenotypic analysis of 300 subjects. Ann Neurol 1999; 46: 224–33.

Ridgway GR, Omar R, Ourselin S, Hill DL, Warren JD, Fox NC. Issues with threshold masking in voxel-based morphometry of atrophied brains. NeuroImage 2009; 44: 99–111.

Ryan NS, Keihaninejad S, Shakespeare TJ, Lejhmann M, Crutch SJ, Malone IB, et al. Magnetic resonance imaging evidence for presymptomatic change in thalamus and caudate in familial Alzheimer's disease. Brain 2013; 136: 1399–414.

Shiga Y, Miyazawa K, Sato S, Fukushima R, Shibuya S, Sato Y, et al. Diffusion-weighted MRI abnormalities as an early diagnostic marker for Creutzfeldt–Jakob disease. Neurology 2004; 63: 443–9.

Sullivan EV, Pfefferbaum A. Diffusion tensor imaging and aging. Neurosci Biohav Rev 2006; 30: 749–61.

Suzuki K, Kawasaki A, Nagashima T, Hirata K. Diffusion-weighted MRI abnormalities antedate the onset of sporadic Creutzfeldt–Jakob disease. Neurology 2016; 87: 843–5.

Thompson AG, Lowe J, Fox Z, Lukic A, Porter MC, Ford L, et al. The Medical Research Council prion disease rating scale: a new outcome measure for prion disease therapeutic trials developed and validated using systematic observational studies. Brain 2013; 136: 1116–27.

Tschampa HJ, Murtz P, Flacke S, Paus S, Schild HH, Urbach H. Thalamic involvement in sporadic Creutzfeldt–Jakob disease: a diffusion-weighted MR imaging study. AJNR Am J Neuroradiol 2003; 24: 908–15.

Vitali P, Maccagnano E, Caverzasi E, Henry RG, Haman A, Torres-Chae C, et al. Diffusion-weighted MRI hyperintensity patterns differentiate CJD from other rapid dementias. Neurology 2011; 76: 1711–9.

Wang Q, Xu X, Zhang M. Normal aging in the basal ganglia evaluated by the eigenvalues of diffusion tensor imaging. AJNR Am J Neuroradiol 2010; 31: 516–20.

Young GS, Geschwind MD, Fischbein NJ, Martindale JL, Henry RG, Liu S, et al. Diffusion-weighted and fluid-attenuated inversion recovery imaging in Creutzfeldt–Jakob disease: high sensitivity and specificity for diagnosis. AJNR Am J Neuroradiol 2005; 26: 1551–62.

Zanusso G, Camporese G, Ferrari S, Santelli L, Bongianni M, Fiorini M. Long-term preclinical magnetic resonance imaging alterations in sporadic Creutzfeldt–Jakob disease. Ann Neurol 2016; 80: 629–32.

Zhang H, Schneider T, Wheeler-Kingshott CA, Alexander DC. NODDI: practical in vivo neurite orientation dispersion and density imaging of the human brain. NeuroImage 2012; 61: 1000–16.